

Why life is hot

Tanja Schilling*

Institute of Physics, University of Freiburg, Hermann-Herder-Straße 3, D-79104 Freiburg, Germany.

Patrick Warren

The Hartree Centre, STFC Daresbury Laboratory, Warrington, WA4 4AD, United Kingdom

Wilson Poon

*School of Physics and Astronomy, The University of Edinburgh,
Peter Guthrie Tait Road, Edinburgh EH9 3FD, United Kingdom.*

(Dated: December 5, 2025)

The process of evolution by natural selection leads to fitness-maximising phenotypes. On the level of cellular chemical reaction networks, maximising fitness can mean optimising a variety of fitness functions such as robustness, precision, or sensitivity to external stimuli. Using theory and numerics, we show that these diverse goals can be achieved by a versatile, generic mechanism: coupling chemical reaction networks to reservoirs that are strongly out of equilibrium. Moreover, we demonstrate that the degree of optimality achievable by this mechanism saturates, and that nature appears to operate near saturation. We find that the amount of heat generated by this mechanism constitutes a significant fraction of the total heat produced by living organisms, so that ‘life is hot’ largely because of the need for a versatile mechanism to optimise a variety of fitness functions.

Introduction

Two features of life are typically taken as self evident: first that it is a non-equilibrium phenomenon, and second that it ubiquitously generates heat.[1] That ‘life is hot’ is considered so banal that it seldom draws comments except in textbooks, although it is striking that the specific heat dissipation of organisms spanning 20 orders of magnitude of body mass stays within a narrow band of $1\text{--}100\text{ W kg}^{-1}$ [2]. By contrast, that ‘life is non-equilibrium’ is frequently discussed, especially in the physics literature [3], because non-equilibrium statistical mechanics continues to pose formidable challenges.

Interestingly, the most common textbook explanation of why life must generate heat, e.g., as given in successive editions of a well-known university text [4], is incorrect. Alberts et al. explain that cellular metabolism generates ‘order’, which lowers entropy. To satisfy the Second Law of Thermodynamics, enough heat must be exported to raise the entropy of the environment to give a net positive entropy change. However, numerical estimates of the total entropy reduction due to various ordering processes within a cell (polymerisation, compartmentalisation, etc.) show that this argument underpredicts the heat production by around two orders of magnitude [5]. Cells reject much more heat than is needed to compensate for their ‘negentropy’ [6]. Why, then, does life ubiquitously produce heat?

Here, we seek to advance our understanding of this issue, and find that at least a substantial part of the answer is deeply entwined with the fact that optimizing

the fitness of living organisms requires non-equilibrium processes. At its most basic level, the claim that life is a non-equilibrium phenomenon applies to intracellular chemical reactions. To quantify a reaction’s degree of ‘disequilibrium’, consider the dimensionless ratio between the equilibrium constant K and the reaction quotient Q , which satisfies $K/Q = \exp(\Delta G/RT)$ where ΔG is the change in the Gibbs’ free energy for the reaction, R is the universal gas constant and T is the temperature.[7]

The degree to which K/Q deviates from unity is therefore a measure of how far a reaction is out of equilibrium. Consider, for example, the 25 highly-conserved reactions making up the glycolysis pathway turning glucose into pyruvate [8] and the tricarboxylic acid cycle that produces high-energy electron carriers from pyruvate to manufacture ATP [9]. Interestingly, only a minority of these 25 reactions are very far from equilibrium: 5 of them show $10^5 < K/Q < 10^7$ (i.e. $\Delta G \simeq 11\text{--}16 k_B T$). Compared to these so-called ‘metabolically irreversible reactions’ [10], 15 of the 25 reactions occur close to equilibrium, $10^{-1} < K/Q < 10^2$ ($\Delta G < 5 k_B T$), with 8 being quasi-equilibrium, $10^{-1} < K/Q < 10^0$ ($\Delta G \simeq 0$).

The most ubiquitous ‘metabolically irreversible reaction’ is the hydrolysis of adenosine triphosphate (ATP) to adenosine diphosphate (ADP) and an inorganic phosphate group, for which $K/Q \simeq 10^9$ for cells in diverse organisms (bacteria, yeast, spinach) under typical living conditions [11]. Hydrolysis of other ‘high-energy nucleoside triphosphates’ such as guanosine triphosphate (GTP) shows similar values. Next to why life produces heat, a second question that we propose to tackle in this work is whether it is necessary for life that a handful of ubiquitous hydrolysis reactions occurs at such high K/Q . Our answer is related to our explanation of why life should typically be hot, because it turns out that both

* tanja.schilling@physik.uni-freiburg.de

issues are intimately related by the ‘logic’ of how intracellular reaction cycles can be optimised for a diverse range of functions.

First, as a preliminary, note that ‘non-equilibrium’ does not necessitate ‘hot’. Indeed, the extraction of $-\Delta G$ useful work from a chemical reaction at constant temperature and pressure may involve *absorbing* heat from its environment. To see this, recall that under quasi-static conditions $Q = T\Delta S = \Delta H - \Delta G$ where (Q, T, S, H) are the (absorbed) heat (not to be confused with the reaction quotient Q), temperature, entropy, and enthalpy respectively. If $\Delta S > 0$ then $Q > 0$ (the quasi-static reaction is endothermic); this is the case for example in the quasi-static oxidation of carbon or glucose under standard conditions [12–14].

Instead, the link between heat generation and a handful of ubiquitous nucleoside triphosphate hydrolysis reactions lies in the evolutionary pressure to optimize chemical reaction networks for a variety of functions. Sometimes organisms need to be precise (e.g. when translating mRNA into proteins), sometimes they need to produce superstructures with tightly-defined properties (e.g. long actin filaments with a narrow length distribution) and sometimes they need to react at speed to external stimuli (e.g. when a heat shock occurs). We now show that adding cycles to chemical reaction networks is a highly versatile way to optimise these networks with respect to a variety of fitness functions, but necessarily generates a significant amount of heat dissipation.

Reaction networks with cycles

To see why cycles are useful, consider first a ‘tree-like’ reaction network without cycles, Fig. 1(a). We denote the reaction rates k_{ij} , where i and j label the chemical species. The state of the system at any given time t is characterized by the concentrations of the species $c_i(t)$ and the currents $J_{ij}(t) := k_{ij}c_j(t) - k_{ji}c_i(t)$. Consider now how we may optimize the steady state of the network with respect to some fitness function $f(c_1, \dots, c_N, J_{11}, \dots, J_{NN})$.

On a tree-like network, steady-state concentration ratios c_i^s/c_j^s are given by the detailed balance condition $J_{ij}^s = k_{ij}c_j^s - k_{ji}c_i^s = 0 \forall i, j$ [15]. To change these ratios, one must either alter one or more rates k_{ij} or add species and therefore reactions to the network.[16] Both occur in living organisms, e.g., via point mutations to extant proteins or the emergence of (say) a novel inhibitor. Either mechanism requires a one-off, specific chemical innovation as each new challenge arises; neither is a suitable ‘design principle’ for a generic solution.

To design a generic solution for optimising networks for multiple fitness functions without changing the chemistry of the constituents, we need to transcend the constraints imposed by detailed balance by including cycles [15]. Figure 1(b) shows two examples. The first is the direct inclusion of a cycle in the reactions between species B, C

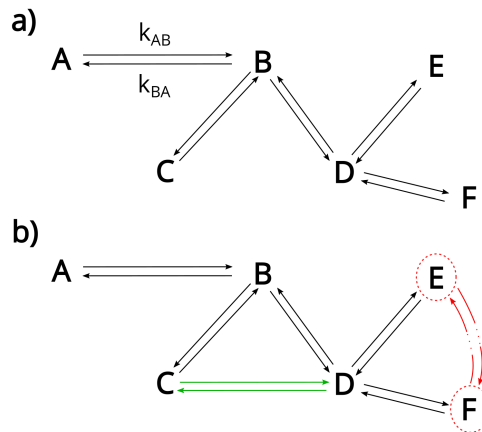


FIG. 1. (a): Tree-like chemical reaction network. (b) Chemical reaction network with cycles. Dashed ellipses denote reservoirs.

and D. The second is less obvious. We have chemiostatted species E and F by particle reservoirs (indicated by the dotted ellipses). In order to keep the concentrations in the reservoirs fixed, there needs to be another chemical reaction network (indicated by the dotted arrows), which closes the cycle.

In a network with cycles, the currents $J_{i,j}^s$ are non-trivial, and it is now possible to tune fitness functions that are not restricted anymore to depend only on the concentrations. In particular, the sensitivities $\frac{\partial \ln c_i^s}{\partial \ln J_{i,j}^s}$ can be optimized [17]. We will show that this explains why cycles are used ubiquitously in biochemistry to tune a variety of different fitness functions, e.g.:

- In protein synthesis the error is reduced with respect to its equilibrium value by means of the Hopfield kinetic proofreading cycle [18–20].
- When heat shock proteins bind to the proteins that they refold, they show ‘ultra-affinity’, i.e. a driven cycle is used to enhance the binding affinity over its equilibrium value [21, 22].
- Cytoskeletal actin filaments have a much sharper length distribution than they would have in equilibrium. [23–25]. Here a driven cycle reduces the polydispersity.
- The sensitivity of chemotaxis is optimized by a cycle that is equivalent in structure to the Hopfield proofreading cycle [26].

The extreme concerns so-called ‘futile’ cycles in which a chemical species is disassembled into its building blocks only to be reassembled again without any obvious purpose [17]. However, if a ‘futile’ cycle is attached to a reaction network, the steady state concentrations are shifted away from their equilibrium values and thus the sensitivity of the network to the boundary conditions is altered.

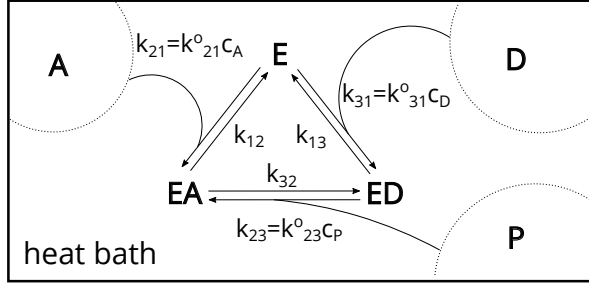


FIG. 2. Reaction network with a heat bath and three chemiostats, which control the concentrations of the species A , D and P .

As has been previously pointed out, the cycle is now *not* at all futile [17] if it is placed at the right node to tune the network's response to variations in currents or concentrations [17, 26–28].

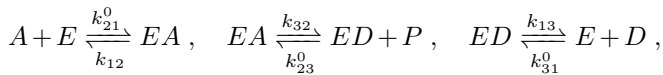
In living organisms, perhaps the most versatile cycles are those involving the hydrolysis of ‘energy currency’ metabolites such as ATP, which are chemiostatted at concentrations very far from their equilibrium values [29] (so that in the DEF cycle in Figure 1(b), E and F may represent ATP and ADP). Such coupling of nucleoside-hydrolysis into cycles is highly versatile; but it comes at a cost that is manifested as a ubiquitous characteristic of life: significant amount of heat is produced.

Dissipation in Chemiostatted Biochemical Networks

To estimate the amount of heat that is produced, consider a chemical reaction network which is attached to three particle reservoirs and embedded in a heat bath at a temperature T , Fig. 2.[30] The system cycles through the states E , EA and ED transporting molecules from the A -reservoir to the D - and P -reservoirs, i.e. the species E acts as a catalyst for the reaction



Species E takes part in three reactions



where k_{ij} are first order rate constants and k_{ij}^0 are second order rate constants, i.e. the corresponding rates are given by products with concentrations such as $k_{21}^0 c_A =: k_{21}$. The cyclic process has to be possible, *inter alia*, in equilibrium. Hence the reaction rates need to fulfill the condition

$$\frac{k_{21}^0 k_{32} k_{13}}{k_{12} k_{23}^0 k_{31}^0} = \frac{c_D^{\text{eq}} c_P^{\text{eq}}}{c_A^{\text{eq}}}, \quad (2)$$

where c_i^{eq} is the concentration of species i in equilibrium.[31]

If we set the concentrations in the A , D and P reservoirs to values other than the equilibrium concentrations, the system runs in a non-equilibrium steady state (NESS). The change of free energy in the NESS is entirely determined by the properties of A , D and P

$$\frac{\Delta G}{k_B T} = \ln \left(\frac{\mathcal{Q}_{APD}}{K_{APD}} \right), \quad (3)$$

where $\mathcal{Q}_{APD} = c_D c_P / c_A$ is the reaction quotient in which c_i denotes the reservoir concentration of particle species i , and the equilibrium constant for Reaction (1) is $K_{APD} = c_P^{\text{eq}} c_D^{\text{eq}} / c_A^{\text{eq}}$.

In the NESS entropy is produced at a rate [20, 28]

$$\begin{aligned} \frac{dS^{\text{sys}}(t)}{dt} &= \frac{k_B}{2} \sum_{i,j \neq i} (k_{ij} c_i^s - k_{ji} c_j^s) \ln \left(\frac{k_{ij} c_j^s}{k_{ji} c_i^s} \right) \\ &= \frac{1}{T} J^s \Delta G, \end{aligned} \quad (4)$$

with $i, j \in \{E, EA, ED\}$. Here we have introduced the steady state current $J^s := \sum_{i,j \neq i} (k_{ij} c_i^s - k_{ji} c_j^s)$ and we used the notation $\frac{dS^{\text{sys}}}{dt}$ for the change in entropy that is not due to heat exchange. (The biochemical literature often follows Prigogine and uses notation $\frac{d_i S(t)}{dt}$ for this quantity [32]. The other part of the change in entropy, which is due to heat exchange, is called ‘‘entropy flow’’ in the literature on stochastic thermodynamics [20, 28].) The steady state current in the cycle has the form

$$J^s := k^s c_E^{\text{tot}}, \quad (5)$$

i.e. it is the product of the total concentration of molecules of the species E , $c_E^{\text{tot}} = (c_E^s + c_{EA}^s + c_{ED}^s)$, with a rate k^s , which is determined by the reaction rates and the concentrations in the reservoirs. (We will return to k^s when we discuss the reason for K/Q being so large, and we give a detailed expression in Eq. (11).)

If the particle reservoirs are kept strictly at constant concentrations, then all of the produced entropy enters the heat bath, i.e.

$$T \frac{dS^{\text{sys}}(t)}{dt} = \frac{dQ}{dt}. \quad (6)$$

If the concentrations in the reservoirs were allowed to fluctuate, some of the entropy would enter the particle reservoirs and would not be detected in a calorimetry experiment.[33] As we are interested in estimating orders of magnitude, we focus on the idealized case of perfect chemiostatting, Eq. (6). We obtain for the rate of heat production in the cycle in Fig. 2

$$\frac{dQ}{dt} = k^s c_E^{\text{tot}} \Delta G. \quad (7)$$

Focus now on cycles in which the chemiostatted species are related to nucleoside phosphate ‘energy currency’, e.g. the species A could be ATP, GTP or complexes

formed with these molecules. Species P would then be the inorganic phosphate ion, and species D would be the corresponding ADP, GDP etc. Depending on the specific ‘currency’, the temperature, pH and other conditions, $K_{APD} \simeq 10^5$ – 10^6 M. [34–36] In cells, the concentration of energy sources containing ATP (or GTP) as well as the concentration of inorganic phosphate is in the millimolar range, while the concentrations of hydrolysed forms (ADP etc.) is typically in the micromolar range. Hence, in a biological organism, the reaction quotient $Q_{APD} = c_{DCP}/c_A$ is of the order 10^{-5} – 10^{-6} M, which corresponds to $K_{APD}/Q_{APD} \sim 10^{10}$ – 10^{12} , or equivalently $\Delta G \simeq 21$ – $28 k_B T \simeq 50$ – 70 kJ mol^{-1} . This is a very large number. After providing some numerical estimates of entropy and heat production in real biochemical reactions mimicked by the network in Fig. 2, we will propose an explanation of why natural selection has ‘tuned’ K_{APD}/Q_{APD} to such large values.

Example (1): actin treadmilling

To estimate the magnitude of entropy production, Eq. (4), for actual biochemistry, consider first actin treadmilling, which has evolved to optimise strongly-peaked length distributions of the actin filaments in cytoskeletons to enable their proper functioning [24, 25, 37–40]). The mechanism by which the polydispersity is reduced is the following: Equilibrium attachment and detachment of molecules at the ends of a chain always leads to a Poissonian length distribution, irrespective of how many different species there are and whether the ends of the chain are equal or not. To change the shape of the length distribution, one needs to add a strongly driven cycle such as the one depicted in fig. 2. In the case of actin, this happens via the hydrolysis of bound F-actin subunits (which correspond to species E). First, G-actin monomers are activated by binding to ATP. Activated monomers are then added to the ‘barbed’ end of a filament ($E \rightleftharpoons EA$). While they are part of the filament they are hydrolyzed ($EA \rightleftharpoons ED$), and finally they drop off at the ‘pointed’ end ($ED \rightleftharpoons E$). As the hydrolysis step is strongly irreversible, the system enters a NESS known as ‘treadmilling’, in which the length distribution is much narrower than it would be in equilibrium [24].

Steady state fluxes in this process are on the order of 10 subunits per second added to/removed from a filament [23, 25, 41]. Hence we expect the heat production rate of a single actin filament to be of the order

$$\left(\frac{dQ}{dt}\right)_{\text{fil.}} = k^s c_E^{\text{tot}} \Delta G \simeq \frac{10 \text{ s}^{-1} \times 60 \text{ kJ mol}^{-1}}{6 \times 10^{23} \text{ mol}^{-1}} \simeq 10^{-18} \text{ W}.$$

There are considerable spatiotemporal variations in actin filament concentration in cells. It is particularly high, $\sim 1 \text{ mM}$, in the lamellipodia of migrating fibroblasts [42, 43]. Assuming that the filaments have a length of order 10^2

subunits [44], we expect to see a heat production of

$$\left(\frac{dQ}{dt}\right)_{\text{lamellipodia}} \simeq 6 \text{ W L}^{-1}, \quad (8)$$

which lies within the range for the specific heat dissipation in a diversity of organisms [2, 45]. Experimental verification of our estimate could perhaps come from calorimetric measurements of, e.g., fragments shed from fish karatocytes that are essentially pieces of ‘pure cytoskeleton’ engaged in lamellopodia-like motion [46].

Example (2): kinetic proofreading

An even more ubiquitous example of a chemiostated cycle is the kinetic proofreading cycle, which regulates the error in translating mRNA to proteins in all organisms [18, 19]. To make numerical estimates, we consider proofreading in *Escherichia coli*, in which case the species E and A correspond to the ribosome and the elongation factor (EF) complex between aminoacyl-tRNA and GTP. In the stationary (non-growing) phase, *E. coli* contains between 5000 and 10000 ribosomes per cell (i.e. about 10^{-20} mol). In the exponential growth phase there are up to 55 000 ribosomes (i.e. about 10^{-19} mol). [47]. The step $EA \rightleftharpoons ED$ consists of GTP activation and hydrolysis. Experimentally-determined rates for the combination of these processes vary between $k_{32} \simeq 25 \text{ s}^{-1}$ [48] and 54 s^{-1} [49]. We know of no measured value of k_{13} , and so will follow the strategy of Zuckerman [50, 51] and use the measured value of k_{12} as an estimate, $k_{13} \simeq k_{12} \simeq 100 \text{ s}^{-1}$ [49]. These constants give a steady state current, (5), of $k^s \simeq 20$ – 35 s^{-1} , which in turn gives a heat production rate per bacterium of

$$\left(\frac{dQ}{dt}\right)_{\text{kinpr}} \simeq \begin{cases} 0.2 \text{ pW/cell} & (\text{exponential phase}), \\ 0.02 \text{ pW/cell} & (\text{stationary phase}). \end{cases} \quad (9)$$

Kinetic proofreading in an actively-growing 1 pg *E. coli* bacterium [52] therefore dissipates

$$\left(\frac{dQ}{dt}\right)_{\text{kinpr}} \simeq 200 \text{ W kg}^{-1}. \quad (10)$$

Actively dividing *E. coli* in various nutrient broths dissipate $\simeq 1$ – 4 pW per cell [53], so that kinetic proofreading is apparently responsible for a not insignificant fraction of this dissipation. This does not seem unreasonable, given that protein synthesis, of which kinetic proofreading is a key component, has been estimated to consume up to two-thirds of the energy budget of an active growing *E. coli* cell [54].

It is instructive to inquire into the origins of the remainder of the $\gtrsim 1 \text{ pW}$ heat dissipation in actively growing *E. coli*. To do so, we consider the process of chemiostatting, i.e. of maintaining the ATP reservoir, for which we turn to two highly-curated models of the

metabolism for *E. coli* developed for use within the framework of flux-balance analysis (FBA) [55] (see Materials and Methods).

For fast-growing *E. coli* (doubling time of order 40–50 min) on a glucose minimal medium under aerobic conditions, we determined the total ATP maintenance demand is 60–80 mmol per gram dry weight (gDW) of biomass, of which 6–10% is for so-called non-growth-associated maintenance (NGAM). Assuming all of this ATP is subsequently hydrolysed in ‘futile’ cycles, this corresponds to a heat production rate of 0.3–0.4 pW per bacterium, which is comparable to the heat produced by kinetic proofreading in exponential growth in (9). A similar conclusion is reached if the NGAM component, contributing 0.02–0.04 pW per bacterium, is interpreted as predicting the heat production in stationary phase. In other words, in both exponential growth and stationary phase, kinetic proofreading appears to make a significant or even dominant contribution to the overall heat production from ‘burning’ ATP.

Note, before proceeding, these estimates are admittedly rather crude, since we use the ATP maintenance demand as a proxy for other currency metabolites like GTP and we neglect for example the existence of overflow metabolism and other ‘sinks’ for the ATP. In principle, the calculation could be refined to include these effects. However, precision to this level is beyond the scope of the present work.

Steady-State Current

Finally, we seek to answer the question of why Nature maintains ΔG for nucleoside triphosphate hydrolysis at such a large value. To do so, we return to the steady state current, Eq. (5). The rate k^s is the difference between the product of the ‘anticlockwise rates’, $k_{21}k_{32}k_{13}$, and the product of the ‘clockwise rates’, $k_{12}k_{23}k_{31}$

$$k^s = \frac{k_{21}k_{32}k_{13} - k_{12}k_{23}k_{31}}{d}, \quad (11)$$

normalized by

$$d = k_{21}k_{32} + k_{32}k_{13} + k_{13}k_{21} + k_{31}k_{23} + k_{23}k_{12} + k_{12}k_{31} + k_{13}k_{12} + k_{21}k_{23} + k_{32}k_{31},$$

where we have set $k_{21} = k_{21}^0 c_A$, $k_{23} = k_{23}^0 c_P$, and $k_{31} = k_{31}^0 c_D$.

If re-phosphorylation of the bound EF complex is negligible ($k_{23}^0 c_P \ll k_{21}^0 c_A$) and re-attachment of the hydrolysed EF complex is also small ($k_{31}^0 c_D \ll k_{21}^0 c_A$), the steady state current approaches

$$J_{\text{lim}}^s = \frac{k_{32}k_{13} c_E^{\text{tot}}}{k_{32} + k_{13} + k_{23}^0 c_P},$$

i.e. it saturates at a value that is independent of the reservoir concentrations c_A and c_D . As a consequence,

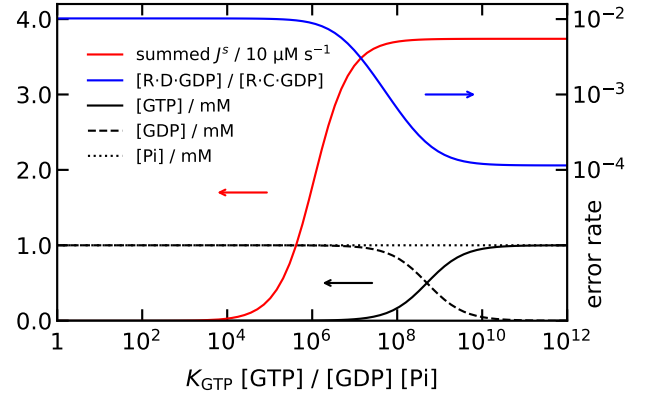


FIG. 3. Kinetic proof reading model: summed cycle flux (red) and error rate (blue), expressed as a function of K/Q for the GTP hydrolysis equilibrium, as the GTP:GDP ratio is varied, constraining $[GTP] + [GDP]$ and $[Pi]$ to 1 mM. (Square brackets indicate concentrations.) Elongation factor complex concentrations are 0.1 mM for both ‘C’ (correct) and ‘D’ (wrong) amino acid types. A copy number of 5000 ribosomes is assumed in a cell volume $2 \mu\text{m}^3$ (concentration $\simeq 4.2 \mu\text{M}$). Detachment rates of the complexes are enhanced by a factor $f = 100$ for the ‘wrong’ amino acid type. For the saturated total cycle flux $J^s/[R]_{\text{tot}} = k^s \simeq 10 \text{ s}^{-1}$, similar to the range quoted in the main text above (9). For more details see Appendix.

the translation error in kinetic proof reading cannot be reduced beyond a certain limit (per proof-reading cycle) [17, 56] and ultra-sensitivity saturates [26]. There is nothing to be gained by bringing the system further out of equilibrium.

To explore this conclusion quantitatively, we implemented a chemiostatted version of a previously-described proofreading model [50, 57], which includes a cycle for the attachment of the correct amino acid to the growing polypeptide chain, as well as a prototypical cycle for the mistaken attachment of a ‘wrong’ amino acid; in the latter the EF complex detachment rates are enhanced. We used rate coefficients and concentrations representative of the situation described above (Appendix).

Figure 3 shows the cycle flux summed over both cycles and the error rate (i.e. the rate of attachment of ‘wrong’ amino acid versus the correct amino acid) as a function of the disequilibrium measure K/Q for $\text{GTP} \rightleftharpoons \text{GDP} + \text{Pi}$. The proofreading effect is clearly seen in the dramatic drop off in the error rate for $K/Q \gtrsim 10^7$. Interestingly, the summed cycle flux (which is dominated by the attachment of correct amino acids) appears to saturate earlier than the proofreading effect. This can be traced to the delayed saturation of the ‘wrong’ attachment cycle. Optimal proofreading thus requires $K/Q \gtrsim 10^{10}$. This simple model therefore explains the physiological requirement for such a large value of ΔG for the fueling currency metabolite (GTP), with the accompanying large heat production arising from its continual consumption.

Conclusion

In his 2025 Nobel Prize lecture Hopfield pointed out: “‘Free energy’ is the key. High-energy molecules like glucose or adenosine triphosphate are expensive for a cell to make, and a biochemical process using unexpectedly large numbers of high-energy molecules in a simple process must be paying that cost for a purpose.” [58]

This argument can be taken further. Most of the energy contained in the currency metabolites is not transformed into chemical work, but dissipated as heat into an organism’s environment. This might seem wasteful at first glance, but we have shown that it provides living organisms with a highly versatile tool to optimize different fitness functions. Nature has driven this mechanism into saturation. In other words, living organisms do not make a compromise between a thrifty use of resources and a moderate improvement of chemical reaction networks. Rather, they take up all the energy needed to run the mechanism optimally, irrespective of the fact that most of the energy is ‘wasted’ as heat. This indicates that from an evolutionary perspective, being able to adapt flexibly to various fitness functions is advantageous over being economical with energy consumption. Life is therefore hot because it is versatile *and* adaptive.

I. APPENDIX

Kinetic proof reading model

To generate the results shown in Fig. 3, we implemented the following model, which hews closely to that described in Refs. [50, 51]. The model comprises quasi-chemical reactions that represent: elongation factor (EF) complex formation (association), $C + GTP \rightleftharpoons C \cdot GTP$; ribosomal binding $R + C \cdot GTP \rightleftharpoons R \cdot C \cdot GTP$; hydrolysis, $R \cdot C \cdot GTP \rightleftharpoons R \cdot C \cdot GDP + Pi$; detachment, $R \cdot C \cdot GDP \rightleftharpoons R + C \cdot GDP$; and dissociation, $C \cdot GDP \rightleftharpoons C + GDP$. All reactions are assumed reversible, though out of equilibrium some are strongly driven in the forward direction. Rate coefficients are, respectively, in the forward and back directions, $g'_t = k_{on} \equiv 10^8 M^{-1} s^{-1}$, $g_t = k_{off} \equiv 100 s^{-1}$; $k' = k_{on}$, $k = k_{off}$; $m' = 0.1 k_{off}$, for m , see below; $l = k_{off}$, $l' = 0.01 k_{on}$; $g_d = 10 k_{off}$, $g'_d = k_{on}$. A so-called ‘cycle constraint’ fixes the value of m in the hydrolysis step according to $m'/m = K_{GTP}(l'/l)(k/k')(g_t/g'_t)(g'_d/g_d)$, where K_{GTP} is the equilibrium constant for the hydrolysis equilibrium $GTP \rightleftharpoons GDP + Pi$; we take $K_{GTP} = 5 \times 10^5 M$ so that $m = 0.02 M^{-1} s^{-1}$. The cycle constraint ensures that the cycle flux vanishes when the concentrations of GTP, GDP and inorganic phosphate (Pi) are at their equilibrium values. We do not explicitly represent polypeptide elongation in the model since it has a very small rate compared to the cycle reactions; rather this step is assumed proportional to the steady-state concentration of the hydrolysed bound EF complex $[R \cdot C \cdot GDP]$.

We also omit direct hydrolysis of GTP and $C \cdot GTP$ since the rates can be assumed negligible under the relevant conditions. Finally, as in Ref. [50], a parallel set of reactions with ‘D’ representing the attachment of a ‘wrong’ amino acid are also included, with detachment rates k and l increased by a factor $f = 100$ compared to ‘C’; the translation error rate is then defined as the ratio $[R \cdot D \cdot GDP]/[R \cdot C \cdot GDP]$. We assume the currency metabolites are chemiostatted as $[GTP] = [G][Pi]/([Pi] + Q_{GTP})$ and $[GDP] = [G]Q_{GTP}/([Pi] + Q_{GTP})$, where $Q_{GTP} = [GDP][Pi]/[GTP]$ is the reaction quotient for the notional GTP hydrolysis equilibrium and $[G] = [GTP] + [GDP]$ is the held-constant phosphorylation-agnostic total concentration of the currency metabolite. To obtain the results shown in Fig. 3, we set the total individual concentrations of C and D at 0.1 mM, calculate the total ribosomal concentration assuming a copy number of 5000 ribosomes in a volume $2 \mu m^3$, take $[G] = [Pi] = 1 mM$ as typical physiological values, and solve for the non-equilibrium steady state (NESS) as a function of the degree of disequilibrium by varying the reaction quotient Q_{GTP} between $5 \times 10^{-7} M$ and the equilibrium upper bound $K_{GTP} = 5 \times 10^5 M$. Different choices here all result in similar phenomenology. We use the BASICO interface [59] to the COPASI simulation platform [60] to perform the actual calculations. A Python script which implements the model and generates Fig. 3 is available on request.

Flux-balance analysis

We used two recent genome-scale metabolic reconstructions, iJO1366 [61] and iML1515 [62], which represent comprehensive models of the metabolic capabilities of *E. coli*, to examine the ATP maintenance demands. We adopted the default growth medium which comprises glucose as the sole carbon/energy source; ammonium, inorganic phosphate and sulfate ions to satisfy the elemental demands for N, P, and S in the biomass; and sundry trace nutrients and minerals unimportant for present purposes. Under aerobic conditions, and limiting the glucose uptake rate to $10 mmol gDW^{-1} hr^{-1}$, we optimise for the flux to biomass using FBA. This yields growth rates of $0.98\text{--}0.88 hr^{-1}$, where here and in the main text the figure for iJO1366 is given first. We then interrogate the models to determine the growth-associated ATP maintenance (GAM) demand incorporated in the flux to biomass, and the non-growth associated ATP maintenance (NGAM) demand associated to the reaction $ATP + H_2O \rightarrow ADP + H^+ + Pi$. Combining these gives the result quoted in the main text. To do the heat production calculation we assume a reaction enthalpy $\Delta H \simeq -30.5 kJ mol^{-1}$ for ATP hydrolysis, take the dry mass of an *E. coli* bacterium as $\simeq 0.43 pg$, and divide by the doubling time to get the quoted heat production rates. The models were downloaded from the BiGG Models database [63], and used as given. FBA calcula-

tions were performed using the COBRApy platform [64]. The Python scripts which perform the calculations are available on request.

ACKNOWLEDGMENTS

WCKP thanks the Isaac Newton Institute for Mathematical Sciences, Cambridge, for supporting participa-

tion in the 2023 ‘New statistical physics in living matter’, where the idea for this work was first conceived. TS thanks the Higgs Centre for Theoretical Physics, The University of Edinburgh, for part funding a sabbatical visit to Edinburgh, where the research was initiated and substantially completed.

-
- [1] Note that a few bacteria apparently absorb heat when they grow [65].
 - [2] A. M. Makarieva, V. G. Gorshkov, B.-L. Li, S. L. Chown, P. B. Reich, and V. M. Gavrilov, Mean mass-specific metabolic rates are strikingly similar across life’s major domains: Evidence for life’s metabolic optimum, *Proc. Natl. Aca. Sci. (USA)* **105**, 16994 (2008).
 - [3] X. Fang, K. Kruse, T. Lu, and J. Wang, Nonequilibrium physics in biology, *Rev. Mod. Phys.* **91**, 045004 (2019).
 - [4] B. Alberts, R. Heald, A. Johnson, D. Morgan, M. Raff, K. Roberts, and P. Walter, *Molecular biology of the cell*, 7th ed. (W.W. Norton & Company, New York, NY, 2022).
 - [5] P. C. Davies, E. Rieper, and J. A. Tuszynski, Self-organization and entropy reduction in a living cell, *Biosystems* **111**, 1 (2013).
 - [6] E. Schrödinger and R. Penrose, *What is Life?: With Mind and Matter and Autobiographical Sketches*, Canto Classics (Cambridge University Press, 2012).
 - [7] Note that other authors, including some cited here, define ΔG with the opposite sign.
 - [8] N. S. Chandel, Glycolysis, *Cold Spring Harb. Perspect. Biol.*, a040535 (2013).
 - [9] C. Chinopoulos, Which way does the citric acid cycle turn during hypoxia? the critical role of alpha-ketoglutarate dehydrogenase complex, *Journal of Neuroscience Research* **91**, 1030 (2013), <https://onlinelibrary.wiley.com/doi/pdf/10.1002/jnr.23196>.
 - [10] L. Moran, R. Horton, G. Scrimgeour, and M. Perry, *Principles of Biochemistry* (Pearson Education, 2011).
 - [11] R. Milo and R. Phillips, *Cell biology by the numbers* (CRC Press, 2015) p. 227.
 - [12] L. Steiner, *Introduction to Chemical Thermodynamics*, 2nd ed. (McGraw-Hill Book Company, 1948).
 - [13] K. G. Denbigh, in *The Principles of Chemical Equilibrium: With Applications in Chemistry and Chemical Engineering* (Cambridge University Press, 1981) p. 73, 4th ed.
 - [14] N. M. Bazhin and V. N. Parmon, Conversion of chemical reaction energy into useful work in the van’t hoff equilibrium box, *J. Chem. Ed.* **84**, 1053 (2007).
 - [15] F. Horn and R. Jackson, General mass action kinetics, *Arch. Ration. Mech. Anal.* **47**, 81 (1972).
 - [16] To see the latter, consider only the network containing species A,B,C,D and E in fig. 1 a). By adding a species F, the concentration of species D can be changed.
 - [17] H. Qian and D. A. Beard, Metabolic futile cycles and their functions: a systems analysis of energy and control, *IEE Proc.: Syst. Biol.* **153**, 192 (2006).
 - [18] J. J. Hopfield, Kinetic proofreading: a new mechanism for reducing errors in biosynthetic processes requiring high specificity, *Proc. Natl. Aca. Sci. (USA)* **71**, 4135 (1974).
 - [19] J. Ninio, Kinetic amplification of enzyme discrimination, *Biochim.* **57**, 587 (1975).
 - [20] H. Boeger, Kinetic proofreading, *Annu. Rev. Biochem.* **91**, 423 (2022).
 - [21] B. Nguyen, D. Hartich, U. Seifert, and P. De Los Rios, Thermodynamic bounds on the ultra-and infra-affinity of Hsp70 for its substrates, *Biophys. J.* **113**, 362 (2017).
 - [22] P. De Los Rios and A. Barducci, Hsp70 chaperones are non-equilibrium machines that achieve ultra-affinity by energy consumption, *eLife* **3**, e02218 (2014).
 - [23] M.-F. Carlier and D. Pantaloni, Control of actin dynamics in cell motility, *J. Mol. Biol.* **269**, 459 (1997).
 - [24] C. Erlenkämper and K. Kruse, Treadmilling and length distributions of active polar filaments, *J. Chem. Phys.* **139** (2013).
 - [25] X. Li, J. Kierfeld, and R. Lipowsky, Actin polymerization and depolymerization coupled to cooperative hydrolysis, *Phys. Rev. Lett.* **103**, 048102 (2009).
 - [26] D. Hartich, A. C. Barato, and U. Seifert, Nonequilibrium sensing and its analogy to kinetic proofreading, *New J. Phys.* **17**, 055026 (2015).
 - [27] H. Qian, Phosphorylation energy hypothesis: open chemical systems and their biological functions, *Annu. Rev. Phys. Chem.* **58**, 113 (2007).
 - [28] D. A. Beard and H. Qian, *Chemical Biophysics* (CUP, Cambridge, UK, 2008).
 - [29] N. Mrnjavac and W. F. Martin, GTP before ATP: The energy currency at the origin of genes, *Biochim. Biophys. Acta, Bioenerg.* **1866**, 149514 (2025).
 - [30] In real biochemistry, such a network will be part of a larger metabolic pathway. We analyze this as a self-contained structure only as a minimal model to estimate heat production in driven reactions.
 - [31] To see this, consider the special case in which the concentrations in the reservoirs are fixed to the equilibrium values of Reaction (1). Then the product of the ratios of forward to backward rates $(k_{21}^0 c_A^{\text{eq}}/k_{12}) \cdot (k_{32}/(k_{23}^0 c_P^{\text{eq}})) \cdot (k_{13}/(k_{31}^0 c_D^{\text{eq}}))$ has to equal 1.
 - [32] D. Kondepudi and I. Prigogine, *Modern Thermodynamics: From Heat Engines to Dissipative Structures*, 2nd ed. (Wiley, 2014).
 - [33] For a discussion of this issue see reference [66], and for an exhaustive analysis of the stochastic thermodynamics of chemical reaction networks with particle reservoirs see reference [67].

- [34] J. Rosing and E. Slater, The value of ΔG° for the hydrolysis of ATP, *Biochim. Biophys. Acta, Bioenerg.* **267**, 275 (1972).
- [35] C. Kötting and K. Gerwert, Time-resolved FTIR studies provide activation free energy, activation enthalpy and activation entropy for gtpase reactions, *Chem. Phys.* **307**, 227 (2004).
- [36] R. A. Alberty, *Thermodynamics of Biochemical Reactions* (John Wiley & Sons, Hoboken, NJ, 2003).
- [37] J.-M. Neuhaus, M. Wanger, T. Keiser, and A. Wegner, Treadmilling of actin, *J. Muscle Res. Cell Motil.* **4**, 507 (1983).
- [38] Z. Hadjivasilou and K. Kruse, Selection for size in molecular self-assembly drives the de novo evolution of a molecular machine, *Phys. Rev. Lett.* **131**, 208402 (2023).
- [39] D. Pantaloni, C. L. Clainche, and M.-F. Carlier, Mechanism of actin-based motility, *Science* **292**, 1502 (2001).
- [40] Z. Hadjivasilou and K. Kruse, Selection for size in molecular self-assembly drives the de novo evolution of a molecular machine, *Phys. Rev. Lett.* **131**, 208402 (2023).
- [41] M.-F. Carlier, Control of actin dynamics, *Curr. Opin. Cell Biol.* **10**, 45 (1998).
- [42] T. D. Pollard, L. Blanchoin, and R. D. Mullins, Molecular mechanisms controlling actin filament dynamics in nonmuscle cells, *Annu. Rev. Biophys. Biomol. Struct.* **29**, 545 (2000).
- [43] V. C. Abraham, V. Krishnamurthi, D. L. Taylor, and F. Lanni, The actin-based nanomachine at the leading edge of migrating cells, *Biophys. J.* **77**, 1721 (1999).
- [44] S. Schaub, J.-J. Meister, and A. B. Verkhovsky, Analysis of actin filament network organization in lamellipodia by comparing experimental and simulated images, *J. Cell Sci.* **120**, 1491 (2007).
- [45] A. M. Makarieva, V. G. Gorshkov, and B. L. Li, Energetics of the smallest: Do bacteria breathe at the same rate as whales?, *Proc. Royal Soc. B* **272**, 2219 (2005).
- [46] A. Mogilner, E. L. Barnhart, and K. Keren, Experiment, theory, and the keratocyte: An ode to a simple model for cell motility, *Semin. Cell Dev. Biol.* **100**, 143 (2020).
- [47] X. Dai, M. Zhu, M. Warren, R. Balakrishnan, V. Patsalo, H. Okano, J. R. Williamson, K. Fredrick, Y.-P. Wang, and T. Hwa, Reduction of translating ribosomes enables *Escherichia coli* to maintain elongation rates during slow growth, *Nat. Microbiol.* **2**, 1 (2016).
- [48] H. S. Zaher and R. Green, Hyperaccurate and error-prone ribosomes exploit distinct mechanisms during tRNA selection, *Mol. Cell* **39**, 110 (2010).
- [49] M. V. Rodnina, K. B. Gromadski, U. Kothe, and H.-J. Wieden, Recognition and selection of tRNA in translation, *FEBS Lett.* **579**, 938 (2005).
- [50] D. Zuckerman, “A Physical Lens on the Cell”: Beginnings of a Free Online Book on Sub-Cellular Biophysical Processes for Students from Heterogeneous Backgrounds, *Biophysical Journal* **106**, 217a (2014).
- [51] D. Zuckerman, Active kinetic proofreading in ‘Physical Lens on the Cell’ online book, <https://physicallensonthecell.org/cell-biology-phenomena/active-kinetic-proofreading> (2015), accessed: 2025-11-29.
- [52] H. Kubitschek and J. Friske, Determination of bacterial cell volume with the Coulter counter, *J. Bacteriol.* **168**, 1466 (1986).
- [53] J. Higuera-Guisset, J. Rodríguez-Viejo, M. Chacón, F. Muñoz, N. Vigués, and J. Mas, Calorimetry of microbial growth using a thermopile based microreactor, *Thermochimica Acta* **427**, 187 (2005).
- [54] O. M. Neijssel, M. J. Teixeira de Mattos, and D. W. Tempest, Growth yield and energy distribution, in *Escherichia coli and Salmonella: cellular and molecular biology*, edited by F. C. Neidhardt, R. C. III, J. L. Ingraham, E. C. C. Lin, K. B. Low, B. Magasanik, W. S. Reznikoff, M. Riley, M. Schaechter, and H. E. Umbarger (American Society for Microbiology, Washington, DC, USA, 1996) 2nd ed., pp. 1683–1692.
- [55] J. D. Orth, I. Thiele, and B. Ø. Palsson, What is flux balance analysis?, *Nature Biotechnology* **28**, 245 (2010).
- [56] A. Murugan, D. A. Huse, and S. Leibler, Speed, dissipation, and error in kinetic proofreading, *Proc. Natl. Aca. Sci. (USA)* **109**, 12034 (2012).
- [57] K. Banerjee, A. B. Kolomeisky, and O. A. Igoshin, Elucidating interplay of speed and accuracy in biological error correction, *Proc. Natl. Aca. Sci. (USA)* **114**, 5183 (2017).
- [58] J. J. Hopfield, Nobel lecture: Physics is a point of view, *Rev. Mod. Phys.* **97**, 030501 (2025).
- [59] F. T. Bergmann, BASICO: A simplified Python interface to COPASI, *J. Open Source Software* **8**, 5553 (2023).
- [60] S. Hoops, S. Sahle, R. Gauges, C. Lee, J. Pahle, N. Simus, M. Singhal, L. Xu, P. Mendes, and U. Kummer, COPASI—a COMplex PATHway Simulator, *Bioinf.* **22**, 3067 (2006).
- [61] J. D. Orth, T. M. Conrad, J. Na, J. A. Lerman, H. Nam, A. M. Feist, and B. Ø. Palsson, A comprehensive genome-scale reconstruction of *Escherichia coli* metabolism—2011, *Mol. Syst. Biol.* **7**, 535 (2011).
- [62] J. M. Monk, C. J. Lloyd, E. Brunk, N. Mih, A. Sastry, Z. King, R. Takeuchi, W. Nomura, Z. Zhang, H. Mori, A. M. Feist, and B. O. Palsson, iML1515, a knowledge-base that computes *Escherichia coli* traits, *Nat. Biotechnol.* **35**, 904 (2017).
- [63] Z. A. King, J. Lu, A. Dräger, P. Miller, S. Federowicz, J. A. Lerman, A. Ebrahim, B. O. Palsson, and N. E. Lewis, BiGG Models: A platform for integrating, standardizing and sharing genome-scale models, *Nucleic Acids Res.* **44**, D515 (2016).
- [64] A. Ebrahim, J. A. Lerman, B. O. Palsson, and D. R. Hyduke, COBRApy: CONstraints-Based Reconstruction and Analysis for Python, *BMC Syst. Biol.* **7**, 74 (2013).
- [65] J.-S. Liu, I. W. Marison, and U. von Stockar, Microbial growth by a net heat up-take: A calorimetric and thermodynamic study on acetotrophic methanogenesis by *methanosarcina barkeri*, *Biotechnology and Bioengineering* **75**, 170 (2001).
- [66] U. Seifert, Stochastic thermodynamics of single enzymes and molecular motors, *Eur. J. Phys. E* **34**, 26 (2011).
- [67] R. Rao and M. Esposito, Conservation laws and work fluctuation relations in chemical reaction networks, *J. Chem. Phys.* **149** (2018).